catalysts

MDPI

Article

Solvent-Free Microwave-Induced Oxidation of Alcohols Catalyzed by Ferrite Magnetic Nanoparticles

Nuno M. R. Martins [1], Luísa M. D. R. S. Martins [1,2,*], Carlos O. Amorim [3], Vitor S. Amaral [3] and Armando J. L. Pombeiro [1]

[1] Centro de Química Estrutural, Instituto Superior Técnico, Universidade de Lisboa, Av. Rovisco Pais, 1049-001 Lisbon, Portugal; nunommartins@tecnico.ulisboa.pt (N.M.R.M.); pombeiro@tecnico.ulisboa.pt (A.J.L.P.)

[2] Chemical Engineering Department, Instituto Superior de Engenharia de Lisboa, Instituto Politécnico de Lisboa, R. Conselheiro Emídio Navarro, 1959-007 Lisboa, Portugal

[3] Department of Physics and CICECO, University of Aveiro, 3810-193 Aveiro, Portugal; amorim5@ua.pt (C.O.A.); vamaral@ua.pt (V.S.A.)

* Correspondence: lmartins@deq.isel.ipl.pt; Tel.: +351-218-419-225 & +351-218-317-226

Received: 28 June 2017; Accepted: 16 July 2017; Published: 24 July 2017

Abstract: A series of first-row-transition-metal ferrite magnetic nanoparticles (NPs) MFe_2O_4 [M = Mn^{2+} (**1**), Fe^{2+} (**2**), Co^{2+} (**3**), Ni^{2+} (**4**), Cu^{2+} (**5**) or Zn^{2+} (**6**)] were prepared by the co-precipitation method and characterized by Fourier transform infrared (FTIR) spectroscopy, powder X-ray diffraction (XRD), scanning electron microscope - energy dispersive X-ray spectrometry (SEM-EDS), vibrating sample magnetometer (VSM) and X-ray photoelectron spectroscopy (XPS). Those NPs were used as catalysts for the microwave-assisted oxidation of various alcohols in solvent-free medium. $MnFe_2O_4$ (**1**), $CoFe_2O_4$ (**3**) and $CuFe_2O_4$ (**5**) act as catalysts for the conversion of alcohols to the corresponding ketones or aldehydes with a yield range of 81 to 94% in 2 h at 120 °C using *t*-BuOOH as an oxidant. These catalysts can be readily isolated by using an external magnet and no significant loss of activity is observed when reused up to 10 consecutive runs. The effects of some parameters, such as temperature, time, type of oxidant and presence of organic radicals, on the oxidation reactions were also investigated. The presented literature overview highlights the advantages of our new **1**–**6** NPs catalytic systems in terms of efficiency and economy, mainly due the used microwave (MW) heating mode.

Keywords: alcohol oxidation; ferrite magnetic nanoparticles; microwave irradiation; solvent-free; recycle

1. Introduction

Nanotechnology knowledge can be applied to improve catalytic organic transformations where a nanometer dimension of a catalyst can enhance its activity, mainly due its high surface area per mass (specific surface area). A type of monodispersed nanomaterials that has been widely explored are spinel ferrites, applied in the fields of information recording, magnetic fluids, drug delivery and in vivo magnetic imaging, due their electronic, optical, electrical, magnetic and catalytic properties, which are different from their bulk counterparts [1–6]. In general, these spinel ferrites, with the standard formula MFe_2O_4, where M is a divalent cation, such as Mn(II), Fe(II), Co(II), Ni(II), Cu(II) or Zn(II), can offer more interesting catalytic activities compared to the corresponding single component metal oxides [7–12].

Catalytic industrial applications of nanoparticles (NPs) have long been a reality [13,14]. Industry tends to favour heterogeneous over homogeneous catalysis due to the advantage of recovery and recycling. In the search for more economic and eco-friendly alternatives, nano-sized spinel ferrites

have significant potential use as a heterogeneous catalyst towards various organic transformations. Especially due to their magnetic properties, a simple and easy catalyst separation and recycling can be applied introducing new synthetic procedures of significance in green chemistry [15].

One of the significant transformations of organic synthesis is the oxidation of alcohols to ketones since the resultant compounds are used in a variety of drugs, agro-chemicals and fragrances. A diversity of methods and oxidants has been developed to accomplish this aim [16,17]. Alcohols have been effectively oxidized by traditional non catalytic methods using stoichiometric quantities of hazardous inorganic oxidizing agents, such as chromium(VI) reagents, permanganates, or *N*-chlorosuccinimide in the presence of mineral acids, which generate large amounts of waste materials [18]. Even grave environmental problems are created using hypervalent iodine reagents [19]. Thus, the development of efficient greener oxidation systems using less poisonous and economic catalysts, oxidants, and solvents under mild conditions became a relevant aim for catalysis.

Heterogeneous protocols have been developed on various supports [20–22]. The search for catalytic oxidation of alcohols in an aqueous medium in the absence of an additional base is still a significant challenge [23]. Among the numerous methods, oxidation of organic species to corresponding carbonyl compounds by O_2, H_2O_2 or *t*-BuOOH, so called "green oxidants", still requires high temperatures and/or long times [24–26], even when using iron oxide NPs as catalysts towards alcohol oxidation [27–30].

In order to improve this type of catalytic system, a valid approach is to turn it into a microwave (MW)-induced catalytic oxidation process, which is about a promising technology for a high activity, especially coupled with appropriate MW absorbent catalysts [31–33]. MW irradiation can provide a much more efficient synthetic protocol than conventional heating towards the production of an added value product, since that similar yields can be obtained in a shorter time and/or the selectivity can be improved [33–40]. In addition, ferrites or materials composed of ferrite powder have attracted a great interest for their strong MW absorption ability, for instance they have been used as absorbing walls for radio waves [41] and for MW-induced degradation of environmental organic contaminants [42]. To the best of our knowledge just iron [29,43,44] and cobalt [30] ferrite types have been studied as catalysts for alcohol oxidation, but no protocol involving MW-irradiation was tested.

Therefore, the performance of spinel ferrites in MW-induced alcohol oxidation deserves to be further investigated. Herewith, we report the synthesis and characterization of several first-row-transition-metal oxide NPs and evaluation of their catalytic performance in the production of ketones or aldehydes by MW-assisted and solvent-free peroxidative oxidation of various alcohol substrates.

2. Results and Discussion

2.1. Catalysts Characterization

2.1.1. FT-IR Spectra (Infrared Spectroscopy)

In the FTIR spectra of **1**–**6** NPs (see the FTIR spectra in Figure S1.1–S1.6), signals related to metal oxide vibrations are observed below 1000 cm^{-1}. The common peak signals below 700 cm^{-1} are due the spinel structure and peaks around 530 cm^{-1} correspond to the intrinsic vibrations of octahedral coordinated metal ions in the spinel structure. This is indicative of the spinel structure in all samples [45].

The **1**–**6** NPs samples also display a broad band signal at ca. 3400 cm^{-1} and a high intensity absorption peak at ca. 1630 cm^{-1}, revealing the presence of hydroxyl groups. Nitrate group symmetric vibrations are detected at ca. 1300 cm^{-1}.

2.1.2. XRD (X-ray Diffraction Pattern)

XRD patterns of **1**–**6** NPs are shown in Figure 1. Considering the angle position and relative intensity, all diffraction peaks were matched against the diffraction files of the Joint Committee on Power Diffraction Standards (JCPDS). In agreement with previous reports [29,42,46], the discernible peaks of **2** NPs were indexed to the lattice planes: (111), (220), (311), (400), (422), (511), (440), (620), (622); resulting to cubic spinel crystalline structure that can be easily indexed to synthetic Fe_3O_4 (JCPDS 79-0417). In contrast **1**, **3**–**6** NPs diffractograms showed no high intensity diffraction peaks which reveals the non-crystalline nature of those NPs. These "atomic disorder" will influence the magnetic properties (see VSM studies below).

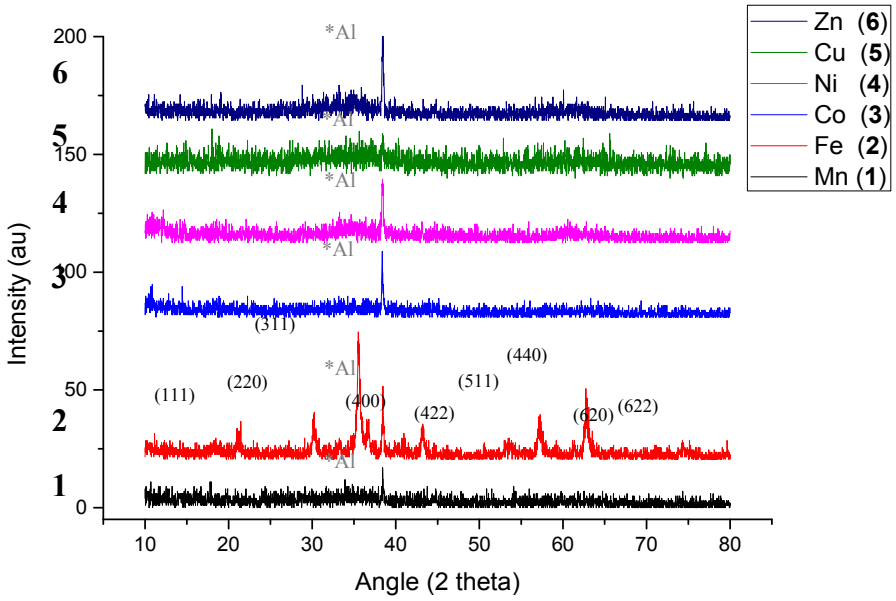

Figure 1. X-ray diffraction patterns of MFe_2O_4 [M = Mn^{2+} (**1**), Fe^{2+} (**2**), Co^{2+} (**3**), Ni^{2+} (**4**), Cu^{2+} (**5**) or Zn^{2+} (**6**)]. * Al—aluminium support sample.

The broad peaks in XRD pattern of **2** NPs are indicative of small size crystallites. The average crystallite size of **2** (22 nm) NPs was determined by considering the full width at half-maximum (FWHM) of diffraction based on Scherrer equation with XRD data ($D = 0.94\,\lambda/\beta\,\cos\theta$, where D is the average particle size of the crystallites, λ is the incident wavelength, θ is the Bragg angle and β is the diffracted full width at half maximum (in radians) caused by crystallization).

2.1.3. TEM (Transmission Electron Microscopy)

TEM micrographs representations of **1**–**6** NPs are shown in Figure 2. With exception of **2**, high level of agglomeration of quasi-spherical particles was observed in all samples. This constituted a limitation towards the statistical study to gather a histogram of the particle size distribution. The prepared NPs have a broad particle size ranging from ca. 4 to 30 nm.

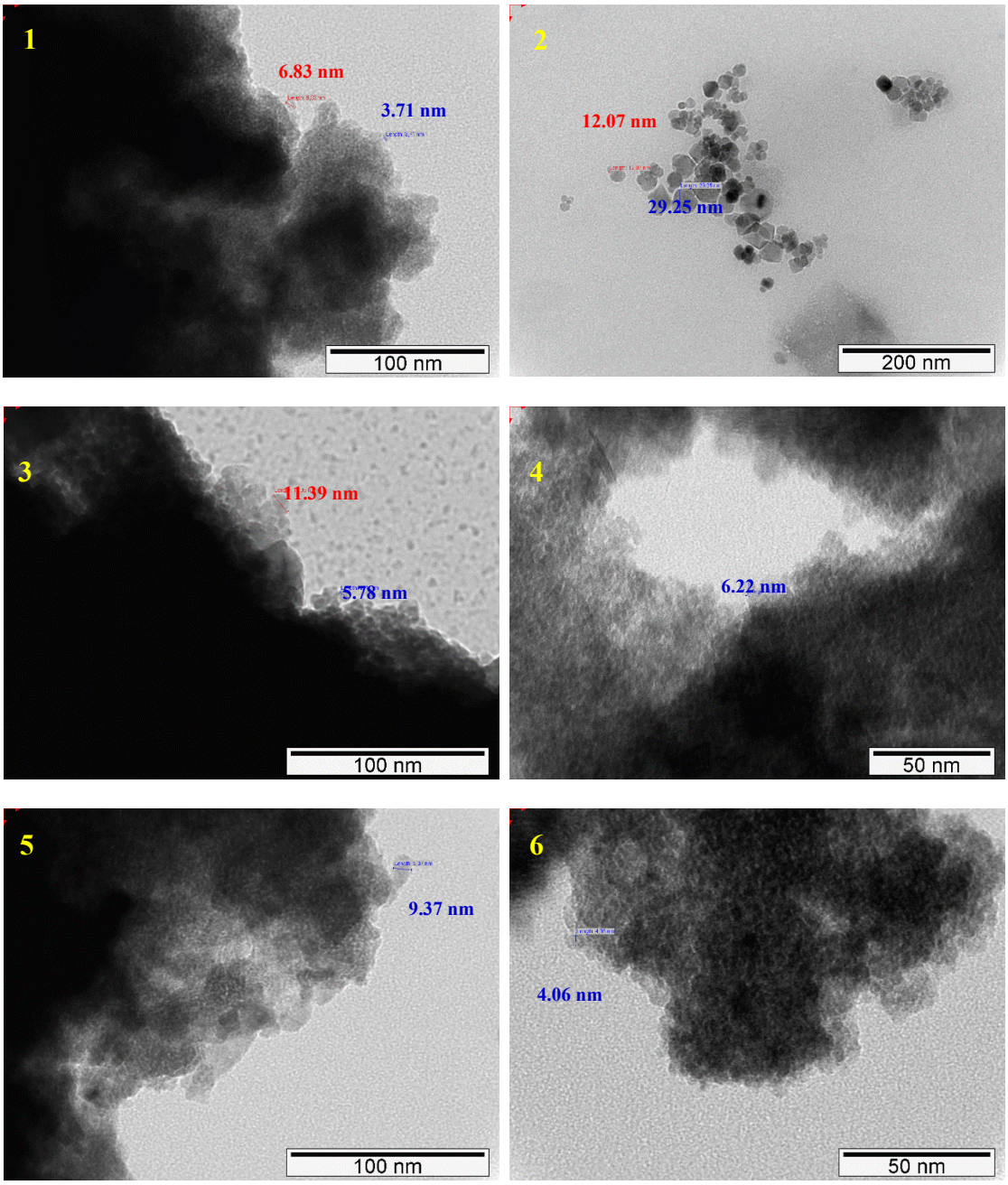

Figure 2. TEM micrographs of MFe_2O_4 [M = Mn^{2+} (**1**), Fe^{2+} (**2**), Co^{2+} (**3**), Ni^{2+} (**4**), Cu^{2+} (**5**) or Zn^{2+} (**6**)].

Representative SEM micrographs of **1**–**6** NPs (Figure 3) exhibit the nanocrystalline irregular spherical shape with the primary size range from ca. 5 to 50 nm. **1** and **2** exhibit at the surface of the materials the lowest size range (5–20 nm) while **4** (5–50 nm) is more aggregated. Regarding **2**, these observations are in accord with the powder XRD obtained data. Moreover, the nanometer scale particles suffer an aggregation effect. This effect in some cases is so massive, such as in **4** NPs, that the combined NPs can form micrometer wide blocks. Despite **1**–**6** NPs were obtained applying the same preparation method the level of aggregation of the formed NPs was widely different. For instance, **1** and **2** NPs show much lower aggregation in comparison with the other prepared NPs.

EDS results confirm that the samples contain only Mn, Fe and O for **1**, Fe and O for **2**, Co, Fe and O for **3**, Ni, Fe and O for **4**, Cu, Fe and O for **5**, Zn, Fe and O for **6** (Figure S2.1–S2.6 and Table S2.1–S2.6).

The atomic ratio Fe/O for **2** was 3:4, and an analogous transition metal ion/Fe/O ratio of 1:2:4 was observed for **1**, **3**–**6**, in agreement with the expected stoichiometry in each case.

2.1.4. SEM–EDS (Scanning Electron Microscopy-Energy Dispersive X-ray Spectroscopy)

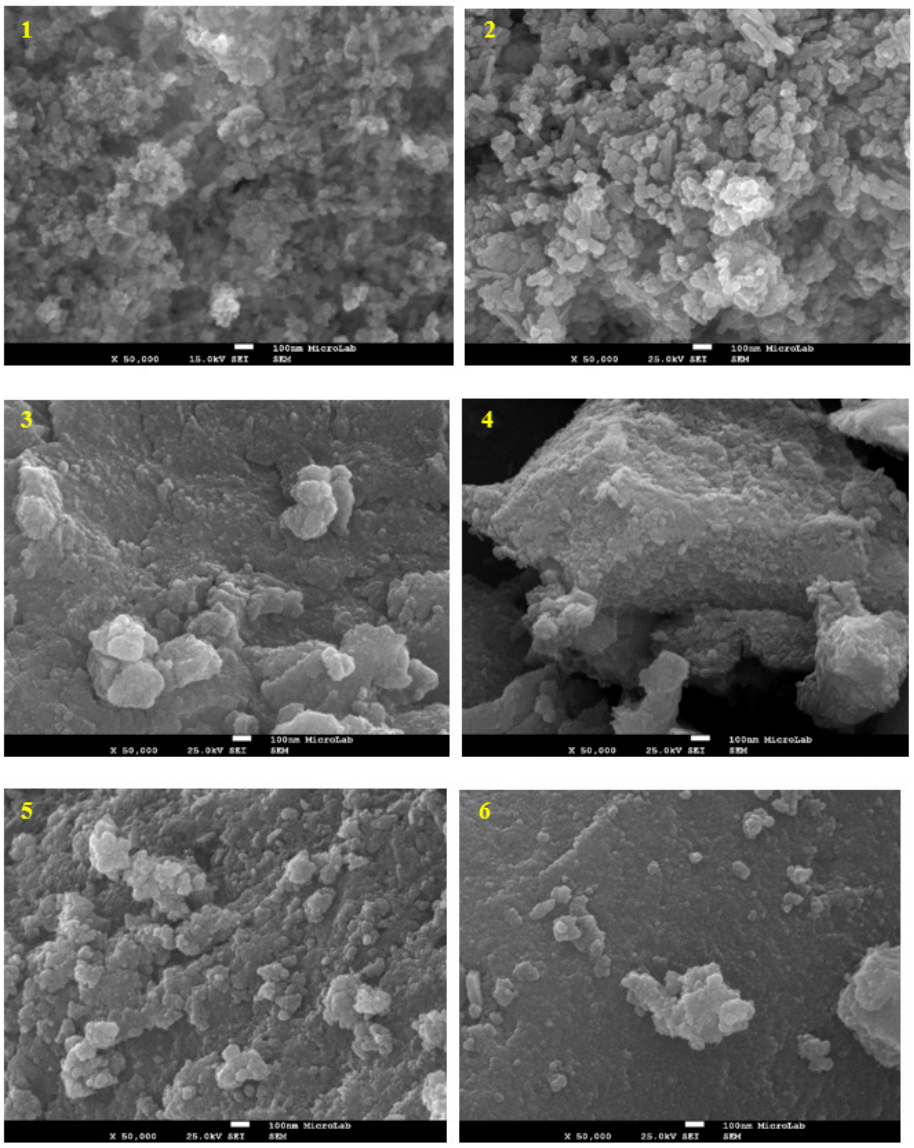

Figure 3. SEM micrographs of MFe_2O_4 [M = Mn^{2+} (**1**), Fe^{2+} (**2**), Co^{2+} (**3**), Ni^{2+} (**4**), Cu^{2+} (**5**) or Zn^{2+} (**6**)].

2.1.5. VSM (Vibrating Sample Magnetometry)

The magnetization (hysteresis cycles) of **1**–**6** NPs as a function of applied field magnetic field was studied by VSM at room temperature in the range $-100 < H < 100$ kOe (Figure 4).

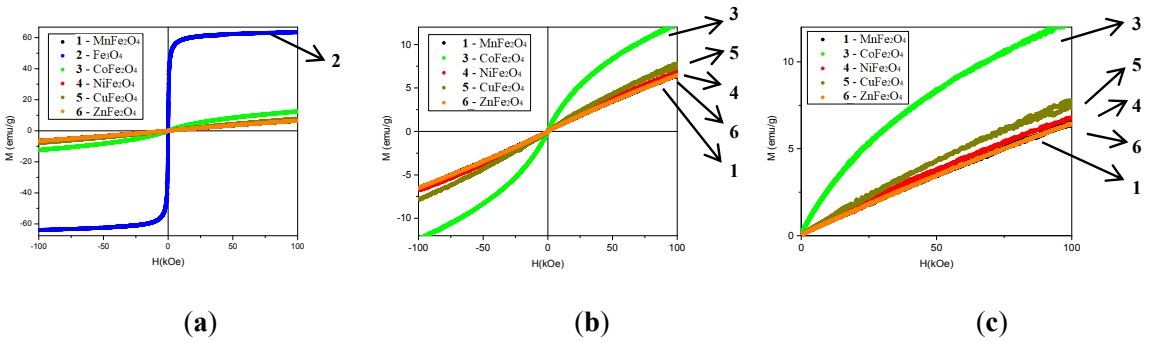

Figure 4. Magnetization curve of MFe_2O_4 [M = Mn^{2+} (**1**), Fe^{2+} (**2**), Co^{2+} (**3**), Ni^{2+} (**4**), Cu^{2+} (**5**) or Zn^{2+} (**6**)]. (**a**): **1**–**6** NPs in the range $-100 < H < 100$; (**b**): **1**, **3**–**6** NPs in the range $-100 < H < 100$; (**c**): **1**, **3**–**6** NPs in the range $0 < H < 100$.

2 NPs are the only ones to present a clear approach to saturation behaviour at 300 K, typical of the ferrimagnetic magnetite Fe_3O_4 bulk phase. The observed maximum magnetization is 63.5 emu/g, comparable to the bulk value, 92.0 emu/g at 300 K [47,48]. The other NPs present a much lower curvature in this field range, being still visible in cobalt **3** NP, much less in the others. In the decreasing order of maximum magnetization at 100 kOe, we have Co, Cu, Ni, Mn and Zn ferrites respectively, as shown in detail for **1**, **3**–**6** NPs (Figure 4).

In general, lower values of magnetization compared to bulk ferrites are common in NPs, being size dependent and usually attributed to non-collinear disordered surface spin arrangements, strong compensation of ionic magnetic moments, due to antiferromagnetic interactions. These are quite dependent on the preparation conditions, which may also lead to different occupancies of spinel sites. An exception is Zn ferrite (**6** NPs), paramagnetic at room temperature in the bulk, but ferrimagnetic in NP or films materials.

All samples present low values of coercive field and remanence magnetization. For **2** NPs the coercive field is 30 Oe, and remanence 2.4 emu/g. In some cases, the cycles are not symmetrical. Such exchange biased behaviour is usually related to surface inhomogeneity and disorder. The cycle widths for other samples are comparable, but with a much lower remanence. As example, **1** exhibits a lower value of maximum magnetization (*Ms* = 6.4 emu/g), while the remanence magnetization and hysteresis cycle width are 10^{-2} emu g^{-1} and 125 Oe, respectively.

2 NPs are the easiest ones to manipulate using an external magnet (Figure 5). Despite **1** has a lower saturation magnetization than **2**, this is enough to allow also the magnetic separation of **1** NPs from the reaction solution with an external magnet. In contrast, **3**–**6** NPs are difficult to separate from the solution relying on their magnetic properties, showing very low response to the external magnet. The aggregation grade on these particular NPs is far greater than on **1**–**2**, as demonstrated by SEM characterization. The magnetization decreases as the particle sizes increases, enhanced by the aggregation effect, due to the inhibition of the surface spin effects.

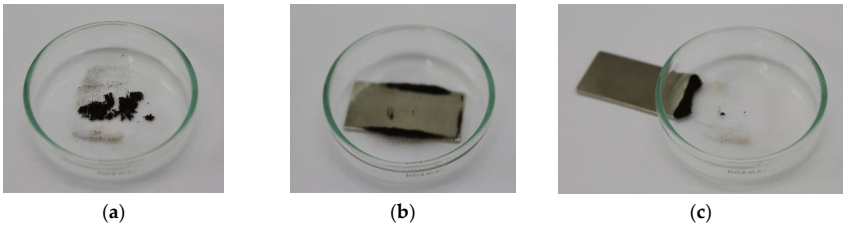

Figure 5. Photographs of the magnetic manipulation of Fe_3O_4 (**2**) Nanoparticles (NPs) using an external magnet. (**a**) In absence of external magnet the **2** NPs are randomly dispersed; (**b**) and (**c**) in presence of external magnet the **2** NPs are grouped by magnetic attraction.

2.2. Catalytic Performance

The **1**–**6** NPs were tested as catalysts for the MW-assisted oxidation of alcohols with *t*-BuOOH in added solvent-free medium. In order to find the optimized reaction conditions, 1-phenylethanol was selected as a model alcohol substrate to oxidize (Scheme 1) and **2** NPs (magnetite) as a model catalyst since it showed the easiest handling among all the prepared NPs, essentially due to its magnetic properties (Figures 4 and 5). Moreover, **2** NPs have been explored towards catalytic reactions, such as alcohol oxidation [6,11,24,26,27,29]. Firstly, the catalytic performance of **2** NPs and its precursor materials was examined in solvent-free medium (Table 1), using *t*-BuOOH as oxidant (chosen because it is a powerful oxidant among peroxidants and in view of the low hazardous grade of the formed by-product *tert*-butyl alcohol). Typically, the reactions were performed with a *t*-BuOOH:1-phenylethanol molar ratio of 2:1, under 10 W MW irradiation, at 80 °C, for 0.5 h. Short time reactions sets are perfect for quick data recovery. Envisaging the quantitative yields achievement moderate-high energy must be fed to the reaction mixture through the raise of temperature. Using a low power MW-irradiation it is ensured that the reaction temperature reaches the selected temperature and can maintain it without significant temperature variations. In all the experiments 1-phenylethanol was oxidized to the corresponding ketone (acetophenone) in a selective manner (>99%).

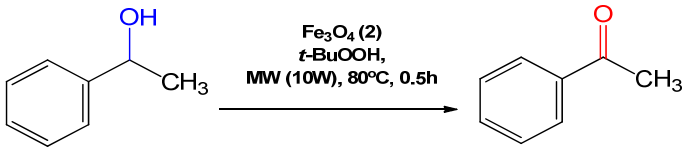

Scheme 1. Solvent-free microwave (MW)-assisted peroxidation of 1-phenylethanol to acetophenone in the presence of *t*-BuOOH using **2** NPs as catalyst.

Table 1. Solvent-free MW-assisted peroxidation of 1-phenylethanol to acetophenone in the presence of various catalysts [a].

Entry	Catalyst	M (mg)	Cat/Alcohol Molar Ratio	Yield [b] (%)
1	none	-	-	1.8
2	$FeCl_2{\cdot}6H_2O$	19.9	0.04	12.9
3	$FeCl_3$	16.2	0.04	22.7
4	$FeCl_2{\cdot}6H_2O$ + $2FeCl_3$	5.3 + 13.3	0.01 + 0.03	15.2
5	Fe_3O_4 (**2**)	2.9	0.005	3.1
6	Fe_3O_4 (**2**)	29.6	0.05	17.8
7 [c]	Fe_3O_4 (**2**)	29.7	0.05	12.2

[a] Reaction conditions: 1-phenylethanol (2.5 mmol), *t*-BuOOH 70% aq. sol., (5.0 mmol), T = 80 °C, MW irradiation (10 W power), t = 0.5 h. [b] Moles of acetophenone per 100 mol of alcohol substrate, selectivity >99%. [c] Carried out under oil bath heating, T = 80 °C.

The blank test in the absence of metal catalyst leads to a very low conversion of 1-phenylethanol to acetophenone (below 2%, Table 1, entry 1). Under the same reaction conditions the iron(II) and iron(III) chlorides were tested using a catalyst/alcohol substrate molar ratio of 0.04, resulting in a higher yield (23%) for the metal salt with the higher oxidation state (Table 1, entry 3). The combination of the two iron salts in a Fe^{3+}:Fe^{2+} ratio of 2:1 (similar ratio in **2** NPs composition) was screened and a lower yield of acetophenone was obtained in comparison with that obtained when the iron(III) salt was used alone (Table 1, entry 4 vs. 3). The ketone yield of 23% (Table 1, entry 3) for $FeCl_3$ could not be surpassed by those for the **2** NPs (3 and 18%, Table 1, entries 5–6). Nevertheless, the use of easily recoverable catalyst can be more desirable, even presenting a lower activity. MW irradiation heating mode lead to a better oxidation reaction efficiency in comparison with the conventional heating mode (Table 1, entries 6 vs. 7).

The oxidation of 1-phenylethanol using **2** NPs was performed in the presence of different oxidizing agents such as atmospheric oxygen, hydrogen peroxide and *tert*-butyl peroxide (Table 2) and, as expected, the highest activity of the catalytic system was achieved with *t*-BuOOH, which proved once more to be more powerful than H_2O_2 towards alcohol oxidation [32]. The attempt to promote the catalytic performance by adding the organic radical 2,2,6,6-tetramethylpiperidin-1-yl)oxidanyl (TEMPO 2.5% mol vs. alcohol substrate) was unsuccessful, resulting in an undesired inhibition effect. The addition of a known C- or O-radical trap, Ph_2NH or $CBrCl_3$ (Table 2, entries 6 and 7, respectively) resulted in a strong inhibition of product formation, indicating the radical reaction nature of the catalytic system using *t*-BuOOH [31,32,40].

Table 2. MW-assisted solvent-free oxidation of 1-phenylethanol using Fe_3O_4 (**2**) as catalyst [a].

Entry	Oxidant	Additive	Yield [b] (%)
§	-	-	no reaction
2	O_2 (1 atm)	-	1.3
3	H_2O_2 30%	-	11.1
4	*t*-BuOOH 70%	-	17.8
5 [c]	*t*-BuOOH 70%	TEMPO 2.5% mol vs. subs	7.3
6 [d]	*t*-BuOOH 70%	Ph_2NH 100% mol vs. subs	0.2
7 [d]	*t*-BuOOH 70%	$CBrCl_3$ 100% mol vs. subs	0.7

[a] Reaction conditions: **2** (30 mg, 0.13 mmol), 1-phenylethanol (2.5 mmol), oxidant agent (5.0 mmol), T = 80 °C, MW irradiation (10 W power), t = 0.5 h. [b] Moles of acetophenone per 100 mol of alcohol substrate, selectivity >99%. [c] Organic radical 2,2,6,6-tetramethylpiperidin-1-yl)oxidanyl (TEMPO, 625 μmol). [d] C and O-radical scavenger compound (2.5 mmol).

The **2** NPs (magnetite) show an inverse cubic spinel structure and the surface shows both Fe^{3+} and Fe^{2+} ions [29,46]. The oxidation of 1-phenylethanol can conceivably occur [31,32] upon hydrogen abstraction by *t*- $BuOO^{\cdot}$ and *t*- $BuO^{\cdot}$ radicals, formed by oxidation or reduction of *t*-BuOOH by Fe^{3+} or Fe^{2+} species at the surface of **2** NPs, respectively (Scheme 2 as an example).

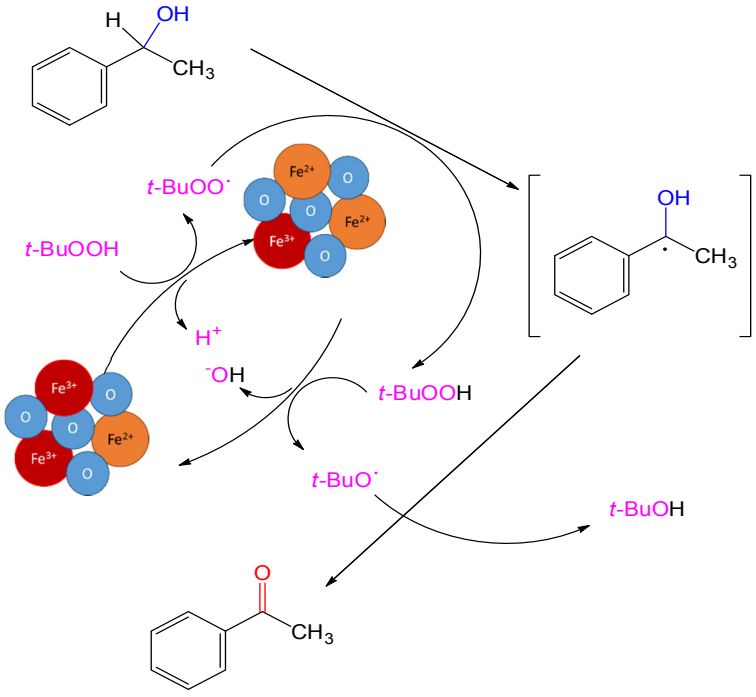

Scheme 2. Proposed catalytic mechanism for Fe_3O_4 (**2**) NPs towards oxidation of 1-phenylethanol to acetophenone in the presence *t*-BuOOH.

Increasing the temperature from 80 to 120 °C results in a yield enhancement, e.g., from 17.8% to 21% (Table 3, entry 2 vs. 4), maintaining the other experimental conditions (2 equiv. of *t*-BuOOH, 0.5 h of reaction time). This increasing activity behaviour along with the temperature rising was expected since temperature has influence in the formation of radical intermediates promoted by the organic peroxidative oxidant [32,36–38,40,49,50]. At 120 °C *t*-BuOOH is more effectively consumed and no increased yield was observed at 150 °C due its self-decomposition at such a temperature. Lower temperatures than 80 °C were also tested (e.g., 50 °C, the lowest temperature allowed by the MW reactor, Table 3, entry 1) leading to low acetophenone yields.

Table 3. MW-assisted solvent-free oxidation of 1-phenylethanol using Fe_3O_4 (**2**) as catalyst [a].

Entry	Temperature (°C)	Yield [b] (%)
1	50	9.2
2	80	17.8
3	100	18.3
4	120	21.2
5	150	18.6

[a] Reaction conditions: **2** (30 mg, 0.13 mmol), 1-phenylethanol (2.5 mmol), oxidant agent (5.0 mmol), MW irradiation (10 W power), t = 0.5 h. [b] Moles of acetophenone per 100 mol of alcohol substrate, selectivity >99%.

After selecting the oxidizing agent (Table 2) and the optimal reaction temperature (Table 3), the effect of the of oxidant/alcohol substrate molar ratio was screened along the reaction time keeping the remaining reaction parameters fixed: catalyst amount (30 mg, 0.13 mmol), 1-phenylethanol (2.5 mmol) and reaction temperature (120 °C). The yields of acetophenone in the different experiments with 2 to 5 equiv. of *t*-BuOOH were compared (Figure 6). As expected changing the oxidant/alcohol substrate molar ratio from 2 to 4 resulted in an increased yield of acetophenone. Using *t*-BuOOH:1-phenylethanol molar ratio of 4 resulted in a 58.3% yield just after 2 h of reaction in contrast to 41.1% yield reached in 3 h with *t*-BuOOH:1-phenylethanol molar ratio of 2. No significant increase of ketone yield was noted in range of 4:1 to 5:1 molar ratio. So, 4 equiv. of *t*-BuOOH vs. alcohol substrate was set as optimal.

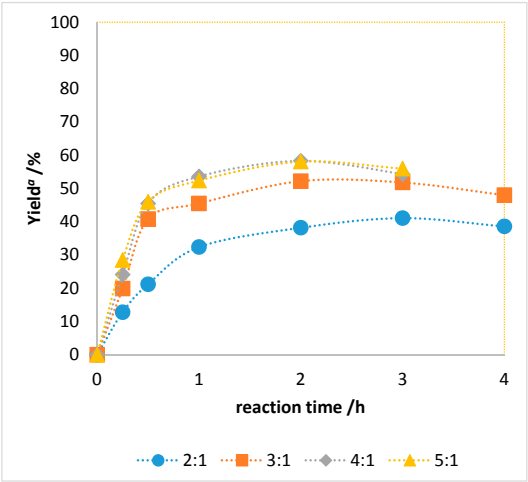

Figure 6. Time reaction studies in MW-assisted solvent-free oxidation of 1-phenylethanol using **2** as catalyst precursors using different oxidant/alcohol substrate ratio. Reaction conditions: 2.5 mmol of 1-phenylethanol; 5 μmol (0.2 mol% vs. substrate) of 2; 5.0, 7.5, 10.0 or 12.5 mmol of *t*-BuOOH (**2**, **3**, **4** or **5** equiv., 70% in H_2O), 0.25, 0.5, 1.0, 2.0, 3.0 and 4.0 h reaction time, 120 °C reaction temperature, MW irradiation (up to 20 W power). [a] Moles of acetophenone per 100 mol of alcohol substrate (GC yield), >99% selectivity.

After established these optimal reaction conditions, a collection of alcohol substrates was further evaluated (Table 4). All the alcohol substrates were oxidized to the corresponding aldehydes or ketones with very high selectivity (>99%), where selectivity is the number of moles of the desired product (aldehyde or ketone) formed by the number of moles of consumed (reacted) substrate. Overoxidation of aldehydes to the corresponding carboxylic acids was not observed. Secondary aromatic alcohols (Table 4, entries 1 and 3) were oxidized in a larger extent than primary ones (Table 4, entries 2 and 4) on account of the higher stability of the radical organic species formed upon hydrogen abstraction (R_2C–OH vs. RHC–OH), in spite of the lower steric hindrance for the latter. Note that the C=C double bond was not affected during the oxidation of cinnamyl alcohol to cinnamaldehyde. The tendency for lower conversion of cyclic aliphatic secondary alcohols in comparison with the aromatic ones can also be explained based on the stability of the radical intermediates in which the aromatic ring play a crucial role. Among the cyclic aliphatic secondary alcohols (Table 3, entries 5–8), the cycloketone yield increases with the ring size (C5 < C6 < C7 < C8), which is in accord with a previous report [40].

Table 4. Solvent-free MW-assisted peroxidation of various alcohols using Fe_3O_4 (**2**) as catalyst [a].

Entry	Substrate	Product	Yield [b] (%)
1	1-Phenylethanol	Acetophenone	58.3
2	Benzyl alcohol	Benzaldehyde	51.2
3	Benzhydrol	Benzophenone	53.5
4	Cinnamyl alcohol	Cinnamaldehyde	38.3
5	Cyclopentanol	Cyclopentanone	39.2
6	Cyclohexanol	Cyclohexanone	41.1
7	Cycloheptanol	Cycloheptanone	45.1
8	Cyclooctanol	Cyclooctanone	46.8

[a] Reaction conditions: catalyst (30 mg, 0.13 mmol), alcohol substrate (2.5 mmol), *t*-BuOOH 70% aq. sol. (10.0 mmol), T = 120 °C, t = 2 h. [b] Moles of acetophenone per 100 mol of alcohol substrate, selectivity >99%.

The activity and selectivity of the NPs should depend upon the metal ions, their oxidation states and their coordination in the lattices, the surface metal cation-oxygen bond strength, the amount of oxygen and morphology of the material [28,42,46].

The reaction conditions, which was refined for **2** NPs catalytic system, can easily be applied to other prepared transition-metal ferrites NPs (**1**, **3**–**6**) for the oxidation of primary and secondary aromatic alcohols (Table 5). It seems that more important than particle size/surface morphology is the nature of the diavalent cation (M^{2+}) of MFe_3O_4 regarding the activity towards benzyl alcohol and 1-phenylethanol oxidation. The higher yields of ketone/aldehyde were obtained with the NPs that possesses the elements Mn (**1**), Co (**3**) and Cu (**5**).

Table 5. Solvent-free MW-assisted peroxidation of 1-phenylethanol and benzylic alcohol using the prepared NPs as catalysts [a].

Catalyst	Acetophenone Yield [b] (%)	Benzaldehyde Yield [b] (%)
$MnFe_2O_4$ (**1**)	80.8	79.1
Fe_3O_4 (**2**)	58.3	51.2
$CoFe_2O_4$ (**3**)	93.7	88.9
$NiFe_2O_4$ (**4**)	52.4	46.2
$CuFe_2O_4$ (**5**)	93.5	86.7
$ZnFe_2O_4$ (**6**)	48.0	44.7

[a] Reaction conditions: catalyst (30 mg, 0.13 mmol), alcohol substrate (2.5 mmol), *t*-BuOOH 70% aq. sol. (10.0 mmol), T = 120 °C, t = 2 h. [b] Moles of ketone or aldehyde per 100 mol of alcohol substrate, selectivity >99%.

Recycling experiments (Figure 7) were carried out under the same optimized conditions with focus only in the prepared NPs with the best catalytic performance, **1**–**3** and **5** NPs (Table 4). These

NPs were reused ten consecutive cycles without a significant decrease in activity. After each reaction only simple magnetic separation and washing with distilled water and ethanol was performed.

In order to get insights about the stability of the tested **1**–**3** and **5** NPs, freshly prepared samples and those after a number of recycles were analysed by XPS. In general, the composition of the analysed NPs remains unchanged (Table S3.1–S3.4 and Figure S3.1–S3.8).

Aiming to show the merit of our developed catalytic system using a series of first-row-transition-metal ferrite magnetic NPs (**1**–**6**) in comparison with other reported methods, it was summarized some of the reported results for the oxidation of benzyl alcohol in Table 6.

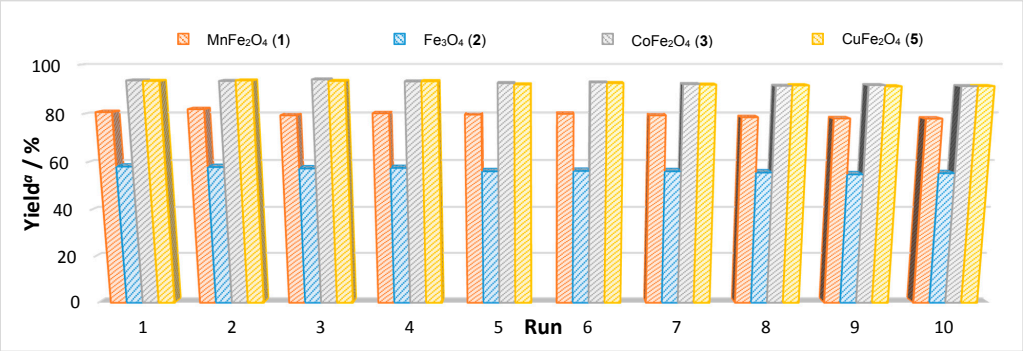

Figure 7. Catalyst recycling in the solvent-free MW-assisted peroxidation of 1-phenylethanol to acetophenone. Reaction conditions: catalyst precursor (30 mg, 0.13 mmol), 1-phenylethanol (2.5 mmol), *t*-BuOOH 70% aq. sol. (10.0 mmol), T = 120 °C, t = 2 h. [a] Moles of acetophenone per 100 mol of alcohol substrate (GC yield), >99% selectivity.

Table 6. Comparison of the oxidation of benzyl alcohol to benzaldehyde using our methodology with other similar reported catalytic systems.

Entry	Catalyst	Reaction Conditions	Conversion [a] (%)	Selectivity [b] (%)	Reference
1	Au/Mg-350	Methanol, 10 atm (O_2), 110 °C, 10 h	96	33	[51]
2	Au/Mg-500	Methanol, 10 atm (O_2), 110 °C, 10 h	78	66	[51]
3	VPO	MeCN, *t*-BuOOH, 90 °C (reflux), 8 h	50	100	[49]
4	VPO-Co-n (0.01)	MeCN, *t*-BuOOH, 90 °C (reflux), 8 h	70	84	[49]
5	VPO-Co-n (0.03)	MeCN, *t*-BuOOH, 90 °C (reflux), 8 h	67	67	[49]
6	VPO-Co-n (0.06)	MeCN, *t*-BuOOH, 90 °C (reflux), 8 h	56	100	[49]
7	VPO-Co-n (0.1)	MeCN, *t*-BuOOH, 90 °C (reflux), 8 h	65	77	[49]
8	VPO-Co-a (0.2)	MeCN, *t*-BuOOH, 90 °C (reflux), 8 h	66	74	[49]
9	VPO-Co-a (0.5)	MeCN, *t*-BuOOH, 90 °C (reflux), 8 h	57	93	[49]
10	VPO-Co-a (1)	MeCN, *t*-BuOOH, 90 °C (reflux), 8 h	66	82	[49]

Table 6. *Cont.*

Entry	Catalyst	Reaction Conditions	Conversion [a] (%)	Selectivity [b] (%)	Reference
11	SIL-$FeCl_3$ (loading $FeCl_3$ = 0.71)	Solvent-free, H_2O_2, 90 °C, 5 h	62.2	70.7	[52]
12	Au@1Pd/SiO_2	Solvent-free, O_2, 90 °C, 6 h	8.8	91	[53]
13	Au@5Pd/SiO_2	Solvent-free, O_2, 90 °C, 6 h	54	93	[53]
14	Au@8Pd/SiO_2	Solvent-free, O_2, 90 °C, 6 h	91	87	[53]
15	Au@10Pd/SiO_2	Solvent-free, O_2, 90 °C, 6 h	88	91	[53]
16	Au@15Pd/SiO_2	Solvent-free, O_2, 90 °C, 6 h	90	88	[53]
17	Au@20Pd/SiO_2	Solvent-free, O_2, 90 °C, 6 h	94	88	[53]
18	$CuAl_2O_4$	MeCN, H_2O_2, 80 °C, 8 h	99	98	[54]
19	AgNPs/rGO	MeCN, NHPI, O_2, 80 °C, 24 h	12	8	[55]
20	Ag NPs/GO	MeCN, NHPI, O_2, 80 °C, 24 h	33	55	[55]
21	Ag NPs/GOSH	MeCN, NHPI, O_2, 80 °C, 24 h	61	58	[55]
22	$CoAl_2O_4$	MeCN, O_2, 80 °C, 5 h	80.9	96.7	[56]
23	CdS-MTA	MeCN, O_2, 5 °C, UV–vis, 1 h	65	>99	[57]
24	Au/HT-3	O_2, in visible light, 24 h	57.4	93.8	[58]
25	Au/HT-3	O_2, in the dark, 24 h	3.7	91.5	[58]
26	Co_2Al-LDH	MeCN, *t*-BuOOH, 60 °C, 30 min	26.9	91.1	[50]
27	$Co_2Mg_{0.5}$Al-LDH	MeCN, *t*-BuOOH, 60 °C, 30 min	38.1	88.9	[50]
28	Co_2MgAl-LDH	MeCN, *t*-BuOOH, 60 °C, 30 min	39.5	89.2	[50]
29	$Co_2Mg_{1.5}$Al-LDH	MeCN, *t*-BuOOH, 60 °C, 30 min	33.8	92.0	[50]
30	Co_2Mg_2Al-LDH	MeCN, *t*-BuOOH, 60 °C, 30 min	32.1	94.9	[50]
31	Pd@PBFS-500	H_2O, O_2, 80 °C, 0.1 MPa, 0.5 h	87	>99	[59]
32	Pd/CB	H_2O, O_2, 80 °C, 0.1 MPa, 2 h	10	>99	[60]
33	Pd/AC	H_2O, O_2, 80 °C, 0.15 MPa, 3 h	18	91	[61]
34	Pd/CMK-3	1,4-Dioxane, O_2, 80 °C, 0.1 MPa, 1 h	55	80	[62]

Table 6. *Cont.*

Entry	Catalyst	Reaction Conditions	Conversion [a] (%)	Selectivity [b] (%)	Reference
35	Pd@hmC	H_2O, K_2CO_3, O_2, 80 °C, 0.1 MPa, 1 h	48	77	[63]
36	Pd/Fe@C	H_2O, K_2CO_3, O_2, 80 °C, 0.1 MPa, 1 h	63	67	[64]
37	Cu-FPZ	MeCN, $NaHCO_3$, TEMPO, O_2, 60 °C, 12 h	99	99	[43]
38	Fe_3O_4	Toluene, O_2, 80 °C, 12 h	80	100	[29]
39	$Fe_3O_4/Cu_3(BTC)_2$	MeCN, Na_2CO_3, TEMPO, O_2, 75 °C, 6 h	>99	>99	[44]
40	$CoFe_2O_4$	Solvent-free, H_2O_2, 110 °C, 5 h	>99	100	[30]
41	$MnFe_2O_4$ (**1**)	Solvent-free, *t*-BuOOH, MW 120 °C, 2 h	79.1	>99	This work
42	Fe_3O_4 (**2**)	Solvent-free, *t*-BuOOH, MW 120 °C, 2 h	51.2	>99	This work
43	$CoFe_2O_4$ (**3**)	Solvent-free, *t*-BuOOH, MW 120 °C, 2 h	88.9	>99	This work
44	$NiFe_2O_4$ (**4**)	Solvent-free, *t*-BuOOH, MW 120 °C, 2 h	46.2	>99	This work
45	$CuFe_2O_4$ (**5**)	Solvent-free, *t*-BuOOH, MW 120 °C, 2 h	86.7	>99	This work
46	$ZnFe_2O_4$ (**6**)	Solvent-free, *t*-BuOOH, MW 120 °C, 2 h	44.7	>99	This work

[a] Conversion of benzyl alcohol (substrate that reacted per 100 mol of substrate). [b] Selectivity based on benzaldehyde (desired product per 100 mol of converted substrate).

To elucidate the merits of **1**–**6** NPs catalytic systems in comparison to the previously reported in literature, Table 6 summarizes the oxidation of benzyl alcohol to benzaldehyde using different catalytic systems. In general, the most active and selective systems use expensive metals, such as gold (entries 1–2,12–17,24–25, Table 6), silver (entries 19–21, Table 6) or palladium (entries 31–36, Table 6). Other transition-metal-based catalysts, such as cobalt (entries 4–10, 22, 26–30, Table 6), iron (entries 11, 38–39, Table 6) or copper (entries 18, 37, Table 6) require organic or/and non-ecofriendly reactants and in most of the cases longer time reaction to reach high conversion and selectivity. Notably, the most similar catalyst to 1–6 NPs, $CoFe_2O_4$ (entry 40, Table 6), presents an excellent catalytic performance. Nevertheless, the present method is more efficient with respect to reaction time and energy consumption (lower heating power due the MW-assisted reaction).

3. Experimental Section

3.1. Materials and Instrumentation

All the chemicals were obtained from commercial sources (Aldrich) and used as received. Infrared spectra (4000–400 cm^{-1}) were recorded on a Vertex 70 (Bruker) instrument in KBr pellets. The catalytic tests under MW irradiation were performed in a focused microwave Anton Paar Monowave 300 reactor (10 W), using a 10 mL capacity reaction tube with a 13 mm internal diameter, fitted with a rotational system and an IR temperature detector. The structural properties of synthesized nanoparticles were analysed by powder X-ray diffraction (PXRD) on a D8 Advance Bruker AXS (Bragg Brentano geometry) theta–2theta diffractometer using Cu (Kα) radiation (wavelength: 1.5406 Å) and a secondary

monochromator, operated at 40 kV and 40 mA at room temperature in the range of 2θ from 10° to 80° with a scan speed of 0.02°/s. The samples were supported on aluminium plaques. The particle size and morphology of the samples were analysed by a transmission scanning electron microscopy (TEM) Hitachi 8100 and scanning electron microscopy (SEM) Hithachi S2400 instrument with Bruker Quantax energy-dispersive X-ray spectroscopy (EDS) and light elements detector. The samples were coated with Au-Pt in an ionization chamber. Magnetic properties were studied using a cryo-free vibrating sample magnetometer (VSM) from Cryogenics that allows measurements in the temperature range 2–320 K, under magnetic fields up to 100 kOe (10 Tesla), with sensitivity and reproducibility of the order 10^{-4} emu, depending on the field range and sweep rate. Gas chromatographic (GC) measurements were carried out using a FISONS Instruments GC 8000 series gas chromatograph with a DB-624 (J&W) capillary column (FID detector) and the Jasco-Borwin v.1.50 software. The temperature of injection was 240 °C. The initial temperature was maintained at 120 °C for 1 min, then raised 10 °C/min to 200 °C and held at this temperature for 1 min. Helium was used as the carrier gas. Reaction products were identified by comparison of their retention times with known reference compounds. The ionic metal content of the ferrite samples was determined by X-ray photoelectron spectroscopy (XPS) using a Kratos Axis Ultra HSA equipment.

3.2. Catalyst Preparation

Ferrite and magnetite nanoparticles were synthesized from an adaptation of a reported co-precipitation method [45]. $FeCl_3$ anhydrous (0.32 g, 2.0 mmol) and $MnCl_2{\cdot}4H_2O$ (0.20 g, 1 mmol) were dissolved in 50 mL deionized water. Ammonia (30% *v*/*v* aq. sol.) was added dropwise till the solution reach pH = 12 while stirring at 80 °C. Then the black turned mixture was cooled to room temperature and was stirred for more 2 h. The precipitate was isolated with the help of an external magnet, washed three times with deionized water, and dried at 60 °C for 6 h.

The above procedure was extended to the synthesis of MFe_2O_4 [M = Mn^{2+} (**1**), Fe^{2+} (**2**), Co^{2+} (**3**), Ni^{2+} (**4**), Cu^{2+} (**5**) or Zn^{2+} (**6**)] NPs by co-precipitation of M(II) and Fe(III) chlorides (M^{2+}/Fe^{3+} = 0.5).

3.3. General Procedure for the Peroxidative Oxidation of Alcohols

In a typical experiment, the alcohol substrate (2.5 mmol), *t*-BuOOH (70% aq. sol., 5.0 mmol) and catalyst **1**–**6** (typically 30 mg) were introduced to a cylindrical Pyrex tube with a magnetic stirring bar, which was then placed in the focused microwave reactor. In the TEMPO-mediated experiments, TEMPO (62.5 μmol, 2.5 mol% vs. substrate) was added to the reaction mixture. The system was stirred and irradiated (10 W) for 15 to 180 min at 80–120 °C. After the reaction, the mixture was allowed to cool down to room temperature. 150 μL of benzaldehyde (or cyclopentanone for the benzyl alcohol oxidation) as internal standard and 2.5 mL of acetonitrile (to extract the substrate and the organic products from the reaction mixture) were added. The obtained mixture was stirred during 10 min and then a sample (0.5 μL) was taken from the organic phase and analysed by GC using the internal standard method.

4. Conclusions

We have introduced a novel straightforward protocol for solvent-free MW-assisted selective oxidation of alcohols to their corresponding carbonyl compounds based in a series of first-row-transition-metal ferrite magnetic nanoparticles with a wide mean size in the 5–50 nm range as heterogeneous catalysts. The advantages of our catalytic systems include the simple preparation of cheap transition metal-based ferrites, use of nontoxic and inexpensive materials, absence of organic solvents, low power (10 W) microwave irradiation for heating, facile separation and recovery of the catalysts from the reaction medium and recyclability (up to ten times) with no significant loss of activity. These features are also advantageous in comparison with previous reports (Table 6). The reaction proceeds via free radicals formation which can be accounted for by reaction of *t*-BuOOH with the metal ions on the surface of the NPs. The order of activity towards the oxidation of 1-phenylethanol of

the studied NPs is $CoFe_3O_4$ (**3**) $\geq$ $CuFe_3O_4$ (**5**) > $MnFe_3O_4$ (**1**) > Fe_3O_4 (**2**) > $NiFe_3O_4$ (**4**) > $ZnFe_3O_4$ (**6**). The application of these NPs to different organic reactions is currently under investigation by us.

Supplementary Materials: The following are available online at www.mdpi.com/2073-4344/7/7/222/s1, Figure S1.1.: FT-IR spectrum of $MnFe_2O_4$ (1) in the range of 4000–400 cm^{-1}, Figure S1.2.: FT-IR spectrum of Fe_3O_4 (2) in the range of 4000–400 cm^{-1}, Figure S1.3.: FT-IR spectrum of $CoFe_2O_4$ (3) in the range of 4000–400 cm^{-1}, Figure S1.4.: FT-IR spectrum of $NiFe_2O_4$ (4) in the range of 4000–400 cm^{-1}, Figure S1.5.: FT-IR spectrum of $CuFe_2O_4$ (5) in the range of 4000–400 cm^{-1}, Figure S1.6: FT-IR spectrum of $ZnFe_2O_4$ (6) in the range of 4000–400 cm^{-1}, Figure S2.1.: EDS spectrum of $MnFe_2O_4$ (1) NPs, Figure S2.2. EDS spectrum of Fe_3O_4 (2) NPs, Figure S2.3.: EDS spectrum of $CoFe_2O_4$ (3) NPs, Figure S2.4.: EDS spectrum of $NiFe_2O_4$ (4) NPs, Figure S2.5.: EDS spectrum of $CuFe_2O_4$ (5) NPs, Figure S2.6.: EDS spectrum of $ZnFe_2O_4$ (6) NPs, Figure S3.1.: Overall XPS spectrum of $MnFe_2O_4$ (1) NPs, Figure S3.2.: XPS spectrum of $MnFe_2O_4$ (1) NPs in regions of interest (ROI), Figure S3.3.: Overall XPS spectrum of Fe_3O_4 (2) NPs, Figure S3.4.: XPS spectrum of Fe_3O_4 (2) NPs in regions of interest (ROI). Figure S3.5.: Overall XPS spectrum of $CoFe_2O_4$ (3) NPs. Figure S3.6.: XPS spectrum of $CoFe_2O_4$ (3) NPs in regions of interest (ROI), Figure S3.7.: Overall XPS spectrum of $CuFe_2O_4$ (4) NPs. Figure S3.8.: XPS spectrum of $CuFe_2O_4$ (4) NPs in regions of interest (ROI), Table S2.1.: Obtained EDS data related to $MnFe_2O_4$ (1) NPs, Table S2.2.: Obtained EDS data related to Fe_3O_4 (2) NPs, Table S2.3.: Obtained EDS data related to $CoFe_2O_4$ (3) NPs, Table S2.4.: Obtained EDS data related to $NiFe_2O_4$ (4) NPs, Table S2.5.: Obtained EDS data related to $CuFe_2O_4$ (5) NPs, Table S2.6.: Obtained EDS data related to $ZnFe_2O_4$ (6) NPs, Table S3.1. XPS data of 1 NPs before and after (8th consecutive run) the peroxidative reaction of 1-phenylethanol, Table S3.2.: XPS data of 2 NPs before and after (5th consecutive run) the peroxidative reaction of 1-phenylethanol, Table S4.3.: XPS data of 3 NPs before and after (7th consecutive run) the peroxidative reaction of 1-phenylethanol, Table S3.4.: XPS data of 4 NPs before and after (5th consecutive run) the peroxidative reaction of 1-phenylethanol.

Acknowledgments: This work has been supported by the Foundation for Science and Technology (FCT), Portugal (UID/QUI/00100/2013, PTDC/QEQ-ERQ/1648/2014 and PTDC/QEQ-QIN/3967/2014 projects). NMRM express gratitude to FCT for the PhD CATSUS fellowship (SFRH/BD/52371/2013). Work was also supported by project CICECO-Aveiro Institute of Materials, POCI-01-0145-FEDER-007679 (FCT Ref. UID/CTM/50011/2013), financed by national funds through the FCT/MEC and when appropriate co-financed by FEDER under the PT2020 Partnership Agreement. The authors thank C.P.M. Sá for the assistance of the XPS analytical services of CEMUP and I. Nogueira for the SEM analysis of MicroLab IST.

Author Contributions: L.M.D.R.S.M. conceived the concept. N.M.R.M designed and performed the experiments. L.M.D.R.S.M. analyzed the data. C.O.A. and V.S.A. performed the VSM studies. L.M.D.R.S.M. and A.J.L.P. provided the means needed for the realization of this work. All the authors contributed to the writing, read and approved the manuscript.

Conflicts of Interest: The authors declare no conflict of interest.

References

1. Caruso, F.; Spasova, M.; Susha, A.; Giersig, M.; Caruso, R.A. Magnetic nanocomposite particles and hollow spheres constructed by a sequential layering approach. *Chem. Mater.* **2001**, *13*, 109–116.
2. Hyeon, T. Chemical synthesis of magnetic nanoparticles. *Chem. Commun.* **2003**, *8*, 927–934. [CrossRef]
3. Zhang, X.X.; Wen, G.H.; Huang, S.; Dai, L.; Gao, R.; Wang, Z.L. Magnetic properties of fe nanoparticles trapped at the tips of the aligned carbon nanotubes. *J. Magn. Magn. Mater.* **2001**, *231*, 9–12.
4. Chiba, D.; Yamanouchi, M.; Matsukura, F.; Ohno, H. Electrical manipulation of magnetization reversal in a ferromagnetic semiconductor. *Science* **2003**, *301*, 943–945. [PubMed]
5. Lu, A.-H.; Schmidt, W.; Matoussevitch, N.; Bönnemann, H.; Spliethoff, B.; Tesche, B.; Bill, E.; Kiefer, W.; Schüth, F. Nanoengineering of a magnetically separable hydrogenation catalyst. *Angew. Chem. Int. Ed.* **2004**, *43*, 4303–4306. [CrossRef] [PubMed]
6. Yan, G.; Jiang, Y.; Kuang, C.; Wang, S.; Liu, H.; Zhang, Y.; Wang, J. Nano-Fe_2O_3-catalyzed direct borylation of arenes. *Chem. Commun.* **2010**, *46*, 3170–3172. [CrossRef] [PubMed]
7. Barbero, B.P.; Gamboa, J.A.; Cadús, L.E. Synthesis and characterisation of La1−xCaxFeO$_3$ perovskite-type oxide catalysts for total oxidation of volatile organic compounds. *Appl. Catal. B Environ.* **2006**, *65*, 21–30. [CrossRef]
8. Xiao, S.H.; Jiang, W.F.; Li, L.Y.; Li, X.J. Low-temperature auto-combustion synthesis and magnetic properties of cobalt ferrite nanopowder. *Mater. Chem. Phys.* **2007**, *106*, 82–87. [CrossRef]
9. Menini, L.; Pereira, M.C.; Ferreira, A.C.; Fabris, J.D.; Gusevskaya, E.V. Cobalt–iron magnetic composites as heterogeneous catalysts for the aerobic oxidation of thiols under alkali free conditions. *Appl. Catal. A Gen.* **2011**, *392*, 151–157.

10. Su, M.; He, C.; Sharma, V.K.; Abou Asi, M.; Xia, D.; Li, X.-Z.; Deng, H.; Xiong, Y. Mesoporous zinc ferrite: Synthesis, characterization, and photocatalytic activity with H_2O_2/visible light. *J. Hazard. Mater.* **2012**, *211–212*, 95–103. [CrossRef] [PubMed]
11. Karami, B.; Hoseini, S.J.; Nikoseresht, S.; Khodabakhshi, S. Fe_3O_4 nanoparticles: A powerful and magnetically recoverable catalyst for the synthesis of novel calix[4]resorcinarenes. *Chin. Chem. Lett.* **2012**, *23*, 173–176. [CrossRef]
12. Conway, B.; Tilak, B. *Advanced Catalysis*; Academic Press: New York, NY, USA, 1992.
13. Cao, H.; Suib, S.L. Highly efficient heterogeneous photooxidation of 2-propanol to acetone with amorphous manganese oxide catalysts. *J. Am. Chem. Soc.* **1994**, *116*, 5334–5342. [CrossRef]
14. Polshettiwar, V.; Varma, R.S. Green chemistry by nano-catalysis. *Green Chem.* **2010**, *12*, 743–754. [CrossRef]
15. Parmeggiani, C.; Cardona, F. Transition metal based catalysts in the aerobic oxidation of alcohols. *Green Chem.* **2012**, *14*, 547–564. [CrossRef]
16. Trost, B.M.; Fleming, I. (Eds.) *Comprehensive Organic Synthesis (Oxidation)*; Pergamon Press: New York, NY, USA, 1991.
17. Sheldon, R.A.; Kochi, J.K. *Metal Catalyzed Oxidations of Organic Compounds*; Academic Press: New York, NY, USA, 1981.
18. González-Arellano, C.; Campelo, J.M.; Macquarrie, D.J.; Marinas, J.M.; Romero, A.A.; Luque, R. Efficient microwave oxidation of alcohols using low-loaded supported metallic iron nanoparticles. *ChemSusChem* **2008**, *1*, 746–750. [CrossRef] [PubMed]
19. Sadri, F.; Ramazani, A.; Massoudi, A.; Khoobi, M.; Tarasi, R.; Shafiee, A.; Azizkhani, V.; Dolatyari, L.; Joo, S.W. Green oxidation of alcohols by using hydrogen peroxide in water in the presence of magnetic Fe_3O_4 nanoparticles as recoverable catalyst. *Green Chem. Lett. Rev.* **2014**, *7*, 257–264. [CrossRef]
20. Mori, K.; Hara, T.; Mizugaki, T.; Ebitani, K.; Kaneda, K. Hydroxyapatite-supported palladium nanoclusters: A highly active heterogeneous catalyst for selective oxidation of alcohols by use of molecular oxygen. *J. Am. Chem. Soc.* **2004**, *126*, 10657–10666. [CrossRef] [PubMed]
21. Lu, T.; Du, Z.; Liu, J.; Ma, H.; Xu, J. Aerobic oxidation of primary aliphatic alcohols over bismuth oxide supported platinum catalysts in water. *Green Chem.* **2013**, *15*, 2215–2221. [CrossRef]
22. Mahyari, M.; Shaabani, A. Graphene oxide-iron phthalocyanine catalyzed aerobic oxidation of alcohols. *Appl. Catal. A Gen.* **2014**, *469*, 524–531. [CrossRef]
23. Sheldon, R.A.; Arends, I.W.C.E.; Hanefeld, U. Catalytic oxidations. In *Green Chemistry and Catalysis*; Wiley-VCH Verlag GmbH & Co. KGaA: Weinheim, Germany, 2007; pp. 133–221.
24. Shi, F.; Tse, M.K.; Pohl, M.-M.; Brückner, A.; Zhang, S.; Beller, M. Tuning catalytic activity between homogeneous and heterogeneous catalysis: Improved activity and selectivity of free nano-Fe_2O_3 in selective oxidations. *Angew. Chem. Int. Ed.* **2007**, *46*, 8866–8868. [CrossRef] [PubMed]
25. Tong, J.; Bo, L.; Li, Z.; Lei, Z.; Xia, C. Magnetic $CoFe_2O_4$ nanocrystal: A novel and efficient heterogeneous catalyst for aerobic oxidation of cyclohexane. *J. Mol. Catal. A Chem.* **2009**, *307*, 58–63. [CrossRef]
26. Gawande, M.B.; Rathi, A.; Nogueira, I.D.; Ghumman, C.A.A.; Bundaleski, N.; Teodoro, O.M.N.D.; Branco, P.S. A Recyclable Ferrite–Co Magnetic Nanocatalyst for the Oxidation of Alcohols to Carbonyl Compounds. *ChemPlusChem* **2012**, *77*, 865–871. [CrossRef]
27. Obermayer, D.; Balu, A.M.; Romero, A.A.; Goessler, W.; Luque, R.; Kappe, C.O. Nanocatalysis in continuous flow: Supported iron oxide nanoparticles for the heterogeneous aerobic oxidation of benzyl alcohol. *Green Chem.* **2013**, *15*, 1530–1537. [CrossRef]
28. De la Hoz, A.; Diaz-Ortiz, A.; Moreno, A. Microwaves in organic synthesis. Thermal and non-thermal microwave effects. *Chem. Soc. Rev.* **2005**, *34*, 164–178. [CrossRef] [PubMed]
29. Shaikh, M.; Satanami, M.; Ranganath, K.V.S. Efficient aerobic oxidation of alcohols using magnetically recoverable catalysts. *Catal. Commun.* **2014**, *54*, 91–93. [CrossRef]
30. Nasrollahzadeh, M.; Bagherzadeh, M.; Karimi, H. Preparation, Preparation, characterization and catalytic activity of $CoFe_2O_4$ nanoparticles as a magnetically recoverable catalyst for selective oxidation of benzyl alcohol to benzaldehyde and reduction of organic dyes. *J. Colloid Interface Sci.* **2016**, *465*, 271–278. [CrossRef] [PubMed]
31. Kopylovich, M.N.; Ribeiro, A.P.C.; Alegria, E.C.B.A.; Martins, N.M.R.; Martins, L.M.D.R.S.; Pombeiro, A.J.L. Chapter three-catalytic oxidation of alcohols: Recent advances. In *Advances in Organometallic Chemistry*; Pedro, J.P., Ed.; Academic Press: Cambridge, MA, USA, 2015; Volume 63, pp. 91–174.

32. Karabach, Y.Y.; Kopylovich, M.N.; Mahmudov, K.T.; Pombeiro, A.J.L. Microwave-assisted catalytic oxidation of alcohols to carbonyl compounds. In *Advances in Organometallic Chemistry and Catalysis*; John Wiley & Sons, Inc.: Hoboken, NJ, USA, 2013; pp. 233–245.
33. Spargo, P.L. Microwave assisted organic synthesis edited by j. P. Tierney and p. Lidstrom. Blackwell Publishing: Oxford. 2005. (Also published by CRC Press in U.S.A. and Canada, ISBN 0-8493-2371-1.). *Org. Process Res. Dev.* **2005**, *9*, 697.
34. Dallinger, D.; Kappe, C.O. Microwave-assisted synthesis in water as solvent. *Chem. Rev.* **2007**, *107*, 2563–2591. [CrossRef] [PubMed]
35. Timokhin, I.; Pettinari, C.; Marchetti, F.; Pettinari, R.; Condello, F.; Galli, S.; Alegria, E.C.B.A.; Martins, L.M.D.R.S.; Pombeiro, A.J.L. Novel coordination polymers with (pyrazolato)-based tectons: Catalytic activity in the peroxidative oxidation of alcohols and cyclohexane. *Cryst. Growth Des.* **2015**, *15*, 2303–2317. [CrossRef]
36. Mahmudov, K.T.; Sutradhar, M.; Martins, L.M.D.R.S.; Guedes da Silva, M.F.C.; Ribera, A.; Nunes, A.V.M.; Gahramanova, S.I.; Marchetti, F.; Pombeiro, A.J.L. Mnii and cuii complexes with arylhydrazones of active methylene compounds as effective heterogeneous catalysts for solvent- and additive-free microwave-assisted peroxidative oxidation of alcohols. *RSC Adv.* **2015**, *5*, 25979–25987. [CrossRef]
37. Sutradhar, M.; Martins, L.M.D.R.S.; Guedes da Silva, M.F.C.; Pombeiro, A.J.L. Oxidovanadium complexes with tridentate aroylhydrazone as catalyst precursors for solvent-free microwave-assisted oxidation of alcohols. *Appl. Catal. A Gen.* **2015**, *493*, 50–57. [CrossRef]
38. Karmakar, A.; Martins, L.M.D.R.S.; Hazra, S.; Guedes da Silva, M.F.C.; Pombeiro, A.J.L. Metal–organic frameworks with pyridyl-based isophthalic acid and their catalytic applications in microwave assisted peroxidative oxidation of alcohols and henry reaction. *Cryst. Growth Des.* **2016**, *16*, 1837–1849. [CrossRef]
39. Liu, X.; An, S.; Shi, W.; Yang, Q.; Zhang, L. Microwave-induced catalytic oxidation of malachite green under magnetic cu-ferrites: New insight into the degradation mechanism and pathway. *J. Mol. Catal. A Chem.* **2014**, *395*, 243–250. [CrossRef]
40. Martins, N.M.R.; Mahmudov, K.T.; Guedes da Silva, M.F.C.; Martins, L.M.D.R.S.; Pombeiro, A.J.L. Copper(II) and iron(III) complexes with arylhydrazone of ethyl 2-cyanoacetate or formazan ligands as catalysts for oxidation of alcohols. *New J. Chem.* **2016**, *40*, 10071–10083. [CrossRef]
41. Maaz, K.; Mumtaz, A.; Hasanain, S.K.; Ceylan, A. Synthesis and magnetic properties of cobalt ferrite ($CoFe_2O_4$) nanoparticles prepared by wet chemical route. *J. Magn. Magn. Mater.* **2007**, *308*, 289–295. [CrossRef]
42. Ghandoor, H.E.; Zidan, H.M.; Khalil, M.; Ismail, M.I.M. Synthesis and some physical properties of magnetite (Fe_3O_4) nanoparticles. *Int. J. Electrochem. Sci.* **2012**, 5734–5745.
43. Hou, J.; Luan, Y.; Yu, J.; Qi, Y.; Wang, G.; Lu, Y. Fabrication of hierarchical composite microspheres of copper-doped Fe_3O_4@P4VP@ZIF-8 and their application in aerobic oxidation. *New J. Chem.* **2016**, *40*, 10127–10135. [CrossRef]
44. Li, J.; Gao, H.; Tan, L.; Luan, Y.; Yang, M. Superparamagnetic Core–Shell Metal–Organic Framework Fe_3O_4/Cu3(btc)2 Microspheres and Their Catalytic Activity in the Aerobic Oxidation of Alcohols and Olefins. *Eur. J. Inorg. Chem.* **2016**, *2016*, 4906–4912. [CrossRef]
45. Deng, H.; Li, X.; Peng, Q.; Wang, X.; Chen, J.; Li, Y. Monodisperse magnetic single-crystal ferrite microspheres. *Angew. Chem. Int. Ed.* **2005**, *44*, 2782–2785. [CrossRef] [PubMed]
46. Soinski, M.; Moses, A.J. Anisotropy in iron-based soft magnetic materials. In *Handbook of Magnetic Materials*; Elsevier: Amsterdam, The Netherlands, 1995; Chapter 4; Volume 8, pp. 325–414.
47. Mattalia, J.M.; Vacher, B.; Samat, A.; Chanon, M. Mechanistic investigation of the reaction between .Alpha.-sulfonyl carbanions and polyhalogenmethanes. Electron transfer versus polar pathways. *J. Am. Chem. Soc.* **1992**, *114*, 4111–4119. [CrossRef]
48. Moiseeva, N.I.; Gekhman, A.E.; Minin, V.V.; Larin, G.M.; Bashtanov, M.E.; Krasnovskii, A.A.; Moiseev, I.I. Free radical/singlet dioxygen system under the conditions of catalytic hydrogen peroxide decomposition. *Kinet. Catal.* **2000**, *41*, 170–182. [CrossRef]
49. Mahdavi, V.; Hasheminasab, H.R. Vanadium phosphorus oxide catalyst promoted by cobalt doping for mild oxidation of benzyl alcohol to benzaldehyde in the liquid phase. *Appl. Catal. A Gen.* **2014**, *482*, 189–197. [CrossRef]

50. Zhou, W.; Liu, J.; Pan, J.; Sun, F.A.; He, M.; Chen, Q. Effect of Mg^{2+} on the catalytic activities of CoMgAl hydrotalcites in the selective oxidation of benzyl alcohol to benzaldehyde. *Catal. Commun.* **2015**, *69*, 1–4. [CrossRef]
51. Estrada, M.; Costa, V.V.; Beloshapkin, S.; Fuentes, S.; Stoyanov, E.; Gusevskaya, E.V.; Simakov, A. Aerobic oxidation of benzyl alcohol in methanol solutions over au nanoparticles: $Mg(OH)_2$ vs. MgO as the support. *Appl. Catal. A Gen.* **2014**, *473*, 96–103. [CrossRef]
52. Cang, R.; Lu, B.; Li, X.; Niu, R.; Zhao, J.; Cai, Q. Iron-chloride ionic liquid immobilized on SBA-15 for solvent-free oxidation of benzyl alcohol to benzaldehyde with H_2O_2. *Chem. Eng. Sci.* **2015**, *137*, 268–275. [CrossRef]
53. Wang, H.; Wang, C.; Yan, H.; Yi, H.; Lu, J. Precisely-controlled synthesis of Au@Pd core–shell bimetallic catalyst via atomic layer deposition for selective oxidation of benzyl alcohol. *J. Catal.* **2015**, *324*, 59–68. [CrossRef]
54. Ragupathi, C.; Judith Vijaya, J.; Thinesh Kumar, R.; John Kennedy, L. Selective liquid phase oxidation of benzyl alcohol catalyzed by copper aluminate nanostructures. *J. Mol. Struct.* **2015**, *1079*, 182–188. [CrossRef]
55. Zahed, B.; Hosseini-Monfared, H. A comparative study of silver-graphene oxide nanocomposites as a recyclable catalyst for the aerobic oxidation of benzyl alcohol: Support effect. *Appl. Surf. Sci.* **2015**, *328*, 536–547. [CrossRef]
56. Ragupathi, C.; Judith Vijaya, J.; Narayanan, S.; Jesudoss, S.K.; John Kennedy, L. Highly selective oxidation of benzyl alcohol to benzaldehyde with hydrogen peroxide by cobalt aluminate catalysis: A comparison of conventional and microwave methods. *Ceram. Int.* **2015**, *41*, 2069–2080. [CrossRef]
57. Tamiolakis, I.; Lykakis, I.N.; Armatas, G.S. Mesoporous CdS-sensitized TiO_2 nanoparticle assemblies with enhanced photocatalytic properties: Selective aerobic oxidation of benzyl alcohols. *Catal. Today* **2015**, *250*, 180–186. [CrossRef]
58. Yu, J.; Li, J.; Wei, H.; Zheng, J.; Su, H.; Wang, X. Hydrotalcite-supported gold catalysts for a selective aerobic oxidation of benzyl alcohol driven by visible light. *J. Mol. Catal. A Chem.* **2014**, *395*, 128–136. [CrossRef]
59. Hao, Y.; Wang, S.; Sun, Q.; Shi, L.; Lu, A.-H. Uniformly dispersed Pd nanoparticles on nitrogen-doped carbon nanospheres for aerobic benzyl alcohol oxidation. *Chin. J. Catal.* **2015**, *36*, 612–619. [CrossRef]
60. Wang, S.; Li, W.-C.; Hao, G.-P.; Hao, Y.; Sun, Q.; Zhang, X.-Q.; Lu, A.-H. Temperature-programmed precise control over the sizes of carbon nanospheres based on benzoxazine chemistry. *J. Am. Chem. Soc.* **2011**, *133*, 15304–15307. [CrossRef] [PubMed]
61. Dimitratos, N.; Villa, A.; Wang, D.; Porta, F.; Su, D.; Prati, L. Pd and pt catalysts modified by alloying with au in the selective oxidation of alcohols. *J. Catal.* **2006**, *244*, 113–121. [CrossRef]
62. Harada, T.; Ikeda, S.; Miyazaki, M.; Sakata, T.; Mori, H.; Matsumura, M. A simple method for preparing highly active palladium catalysts loaded on various carbon supports for liquid-phase oxidation and hydrogenation reactions. *J. Mol. Catal. A Chem.* **2007**, *268*, 59–64. [CrossRef]
63. Harada, T.; Ikeda, S.; Hashimoto, F.; Sakata, T.; Ikeue, K.; Torimoto, T.; Matsumura, M. Catalytic activity and regeneration property of a Pd nanoparticle encapsulated in a hollow porous carbon sphere for aerobic alcohol oxidation. *Langmuir* **2010**, *26*, 17720–17725. [CrossRef] [PubMed]
64. Zhang, H.; Liu, Y.; Zhang, X. Selective oxidation of benzyl alcohol catalyzed by palladium nanoparticles supported on carbon-coated iron nanocrystals. *Chin. J. Catal.* **2011**, *32*, 1693–1701. [CrossRef]